

Electronic Realization of Chaotic Differential Equations

Travis Petersen, Chris Parker, Eric Kangas, Sami Abdul-Wahid, Evan Masters, David Cross, James Mullen, Kendall Taylor and Michael Braunstein (Faculty Advisor)

Physics Department, Central Washington University, Ellensburg, WA 98926

(Submitted 6/30/2008)

Abstract: Using the Undergraduate Research Award provided by the national office of the Society of Physics Students, the CWU chapter of SPS investigated electronic realizations of chaotic systems. The CWU chapter of SPS selected this topic to advance its members' understanding of chaotic systems. J.C. Sprott [2] reported on a class of chaotic differential equations that can, in principle, be simply realized using discrete electronic components. These circuits can be used to experimentally investigate chaotic behavior in a simple system. This report presents a comparison of the computational and experimental data collected from one simple chaotic circuit realizing the differential equation:

$$\ddot{x} = -\alpha\dot{x} - \dot{x} - x + x^2.$$

I. Introduction

Although there exists no universal consensus on an exact definition, chaos is usually described as a deterministic system that displays aperiodic, long-term bounded behavior with sensitive dependence on initial conditions [1]. An interesting class of chaotic differential equations has been found that can be modeled by simple electronic circuits [2], and one of these is the focus of this project. The general form of these equations is given by:

$$\ddot{x} = \alpha\ddot{x} + \beta\dot{x} + \gamma x + f(x) + C,$$

Equation 1

where the dots represent derivatives with respect to time, α , β , γ and C are real constants, and $f(x)$ is a nonlinear function. Because these systems have a dependence on the third time derivative of the variable x , they are identified as jerk functions. When realizing these equations electronically, values of x and its derivatives are characterized by voltages at specific points in the circuit.

We designed and constructed several implementations of circuits for one of these equations:

$$\ddot{x} = -\alpha\ddot{x} - \dot{x} - x + x^2,$$

Equation 2

with a control parameter (α) corresponding to an adjustable electronic component that could be varied to produce a wide range of values. For certain values of the control parameter, the output values vary periodically with time, but if the control parameter is set to a value in the chaotic range, the output values vary in an apparently chaotic manner.

We note that the third order differential equation shown in Equation 2 can be rewritten as three coupled first order differential equations:

$$\begin{aligned}\dot{x} &= y \\ \dot{y} &= z \\ \dot{z} &= -\alpha z - y - x + x^2\end{aligned}$$

Equation 3

In the form of Equation 3, the time evolution of the system can be visualized as a trajectory in a three dimensional space (phase space) with coordinates x , y and z .

With these circuits, we investigated qualitative and quantitative behaviors of the system as a function of the control parameter and compared these behaviors to numerical models.

II. Methods

A. Designing the Circuit

Recognizing that a simple implementation of an integrating circuit consists of a signal applied to the inverting input of an operational amplifier through a resistor, and with feedback applied by a capacitor [3], we designed our circuit, applying the integrator-adder-gain block diagram approach [4]. This allowed us to systematically assemble a circuit using simple operational amplifier circuits to represent different elements of the equation to be realized. Figure 1 shows our final circuit. Early on in the circuit design, we decided to use a variable resistance to realize the control parameter, α .

All of the circuits that were used in this research were constructed (breadboarded) on E&L Instruments C.A.D.E.T.TM electronics trainers. In an initial implementation, the components we used were AD741 [4] operational amplifiers, lower accuracy (5%) resistors and ceramic disc capacitors. In a second implementation, intended to improve the correspondence between the numerical model and the electronic circuit, we used CA3140 operational amplifiers, which have significantly higher input impedance than the AD741 operational amplifiers, and higher accuracy (1%) resistors and polypropylene capacitors [5].

A fundamental aspect of a continuous chaotic system is that it must contain a non-linear term. The x^2 term in Equation 2 is the non-linear term for our system and we implemented this in our circuit using an AD734, 10 MHz, 4-Quadrant Multiplier/Divider integrated circuit in the Basic Multiplier Circuit configuration [6]. The control parameter, α , was implemented through a gain applied to the voltage corresponding to \dot{x} with an operational amplifier circuit in the simple inverting amplifier configuration [3]. In order to automate control and data collection for our circuit we designed this element so that its gain was determined by a feedback resistance that could be controlled through an applied voltage. To accomplish this we used LM13700 dual operational transconductance amplifiers configured as floating voltage controlled resistors [7].

In the second implementation of the circuit we found that some important additional measures were necessary to reduce parasitic oscillations of the CA3140

operational amplifiers: these included using $0.1 \mu\text{F}$ bypass capacitors applied to each operational amplifier power supply lead; and 100Ω damping resistors applied to each operational amplifier power supply lead [8].

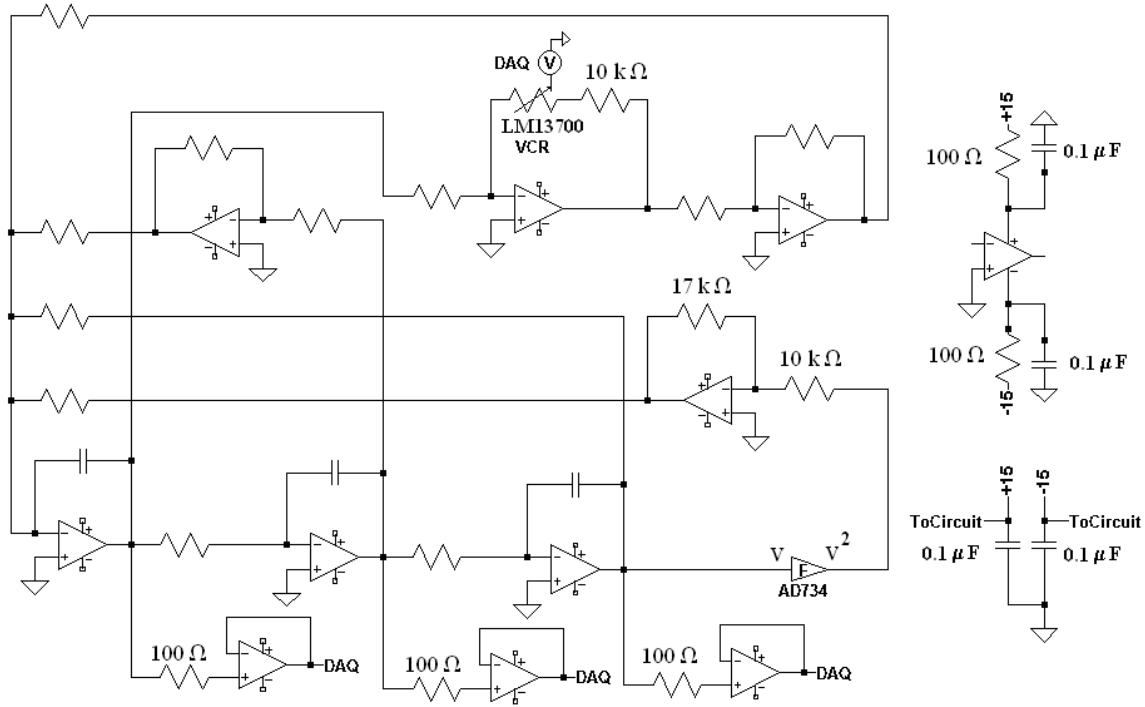


Figure 1: This schematic shows our final implementation of the circuit representing Equation 2. All op-amps are CA3140's, all resistances are $100\text{k}\Omega \pm 1\%$, and all capacitances are $1\text{nF} \pm 1\%$ unless otherwise labeled. The three op-amps configured as buffer/followers connected to the DAQ at the bottom of the schematic are present to minimize the loading effect of the DAQ on the circuit. The voltages present at the outputs of these three buffer/followers represent the three coordinates of phase space from Equation 3. The output of the rightmost buffer/follower represents x , the output of the central buffer/follower represents y , and the output of the leftmost buffer/follower represents z . Op-amp circuits with capacitor feedback are integrating circuits, while op-amp circuits with resistor feedback introduce gain factors (including inversion) to voltages applied to them. The op-amp circuit with the VCR feedback circuit represents the factor α of the first term in our realized equation, and the control voltage for the VCR was applied with an analog output voltage from the DAQ. External components for the LM13700 VCR and the AD734 V^2 circuits are NOT shown in this schematic – as noted in the text, these components and their configurations were consistent with schematics from the respective Data Sheets [6,7]. The diagrams at the right of the schematic show configuration of the bypass capacitors and damping resistors used to reduce parasitic oscillations and noise.

B. Scaling

An analysis of the circuit in Figure 1 using the Op-Amp Current Rule and the Op-Amp Voltage Rule [3] produces the differential equation:

$$(RC)^3 \frac{d^3V}{dt^3} = -\alpha(RC)^2 \frac{d^2V}{dt^2} - RC \frac{dV}{dt} - V + bV^2,$$

Equation 4

where R and C are the common resistance and capacitance used in the integrator-adder-gain portions of the circuit, α is the control parameter adjusted through the control voltage applied to the VCR, V is the voltage at the output of the rightmost buffer/follower in Figure 1, and b is a gain determined by the components and parameters of the squaring portion of the circuit (the AD734).

Comparing Equation 4 with Equation 2, we see that there are factors present in the differential equation describing the circuit that are not associated with the differential equation we are investigating. In fact, though, the presence of these factors can be exploited in the design of the circuit. To see this, we define:

$$\tau = \frac{t}{RC}, \text{ and } v = bV$$

Equation 5

then multiply Equation 4 by a factor of b , and rewrite it in terms of b and τ . We find that the differential equation for v as a function of τ is now identical to the form of Equation 2. That is, the product RC acts as a time scaling for the circuit behavior (in our case, allowing the circuit to operate at frequencies convenient for data sampling) and the gain b acts as an amplitude scaling factor (in our case, allowing the circuit to be operated at amplitudes to enhance the best signal to noise ratio while avoiding amplifier saturation.)

C. Data Acquisition

Data was collected using the **National Instruments 6251 M-Series Data Acquisition hardware (DAQ) device, which was purchased for this project through the SPS Undergraduate Research Award funding.** In addition, the data collection was automated by varying the control parameter through an analog voltage applied to the VCR shown in Figure 1 using an analog output channel of the NI-6251. LabVIEW programs were developed to carry out the circuit automation and data acquisition functions. The principal LabVIEW data acquisition program would scan through a range of control parameters, and at each value of the control parameter sample sets of ordered triplets corresponding the x , y and z coordinates in phase space of Equation 3. Each data set is saved when it is collected and then tagged with the VCR control voltage at which it was collected.

These data sets were used to generate parametric phase plots of the three voltages in our circuit corresponding to x , y , and z of Equation 3 at specific values of the control parameter. These 3 dimensional phase plots represent a complete characterization of the attractor. The data sets were also used to analyze the Lyapunov exponent spectrum for Equation 2 with a routine developed in *Mathematica 6* [10].

A number of additional LabVIEW/NI DAQ applications were developed in the course of this project, including investigations of the control voltage dependence and

frequency dependence of the LM13700 VCR and correlation of the VCR control voltage with the control parameter α from Equation 2.

D. Modeling

To gain understanding of the behavior of Equation 2 and to identify interesting and appropriate parameters in which to carry out the data acquisition portion of the project, we engaged in an extensive program of modeling using *Mathematica 6*. These investigations included:

1. numerical solution of the differential equation in Equation 2 for a broad range of control parameters, scaling dynamics and for different initial conditions
2. graphical representation of the time series corresponding to x , y , and z from Equation 3 using the solutions from 1 above
3. parametric graphical representation of the phase space (the attractor) using the solutions from Equation 1 above
4. investigation of the Lyapunov exponent spectrum using the methods described in [1], which quantitatively characterizes behavior of a chaotic system
5. generation of return maps for a range of control parameters
6. investigation of the eigenvalues of the Jacobian at the fixed points for Equation 3

E. Experimental Lyapunov Spectrum

Using the method described by Rosenstein, et. al. [9], a *Mathematica 6* algorithm was developed to calculate the Lyapunov exponent from time series data. We first calculated the Lyapunov spectrum for time series generated by a computational model to establish that the algorithm was correctly implemented. Comparison of this spectrum with the results described in section III. B. below strongly suggested that the algorithm was correctly implemented.

This algorithm was then applied to data sets collected with the DAQ board as described in section II.C. above to generate an experimental Lyapunov exponent spectrum.

III. Results

A. Modeling Solutions to the Differential Equation

Using *Mathematica 6* to numerically approximate Equation 2, a time series was generated and is shown in Figure 2.

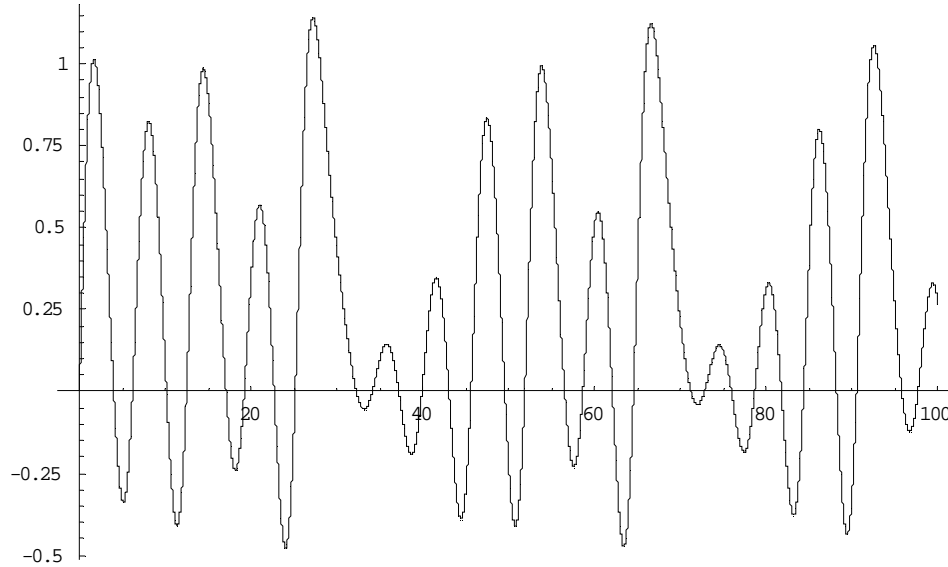


Figure 2: This time series was created by numerically approximating Equation 2 and mapping the solution to x over 100 seconds.

In addition, two and three dimensional phase space diagrams could be created from Equation 3 for any value of the control parameter. Examples of these are shown in Figures 3 and 4 with chaotic and periodic behavior. The *periodic* phase space diagrams in Figures 3 and 4 correspond to a prominent and reproducible periodic feature in the behavior of our system, both for numerical models and the experimental system. When the control parameter values are changed slightly from those that give this periodic behavior, the system behaves chaotically. Such “period windows” are a universal feature of chaotic systems [1]. Because this particular period window was so prominent and reproducible in our system we focused much of our data collection and analysis in a region of the control parameter that contained it. In the remainder of this report we refer to this specific feature as the “period 3 window”.

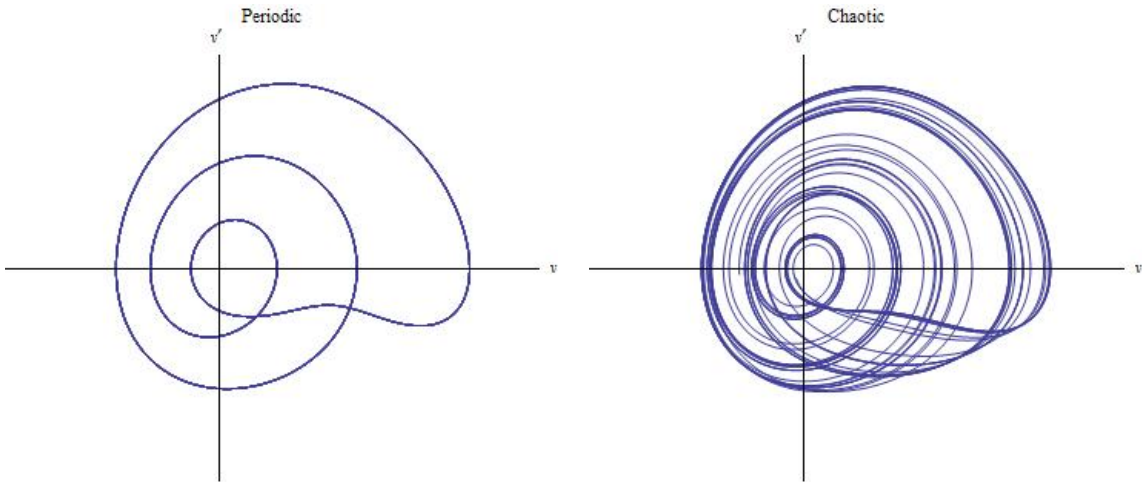


Figure 3: Two dimensional phase space diagrams created by allowing the orbit to evolve from the same initial conditions, for the same amount of time. Using a control parameter of 0.5061, we see periodic behavior (period 3 window, left) and using a control parameter of 0.5035, chaotic behavior is seen (right).

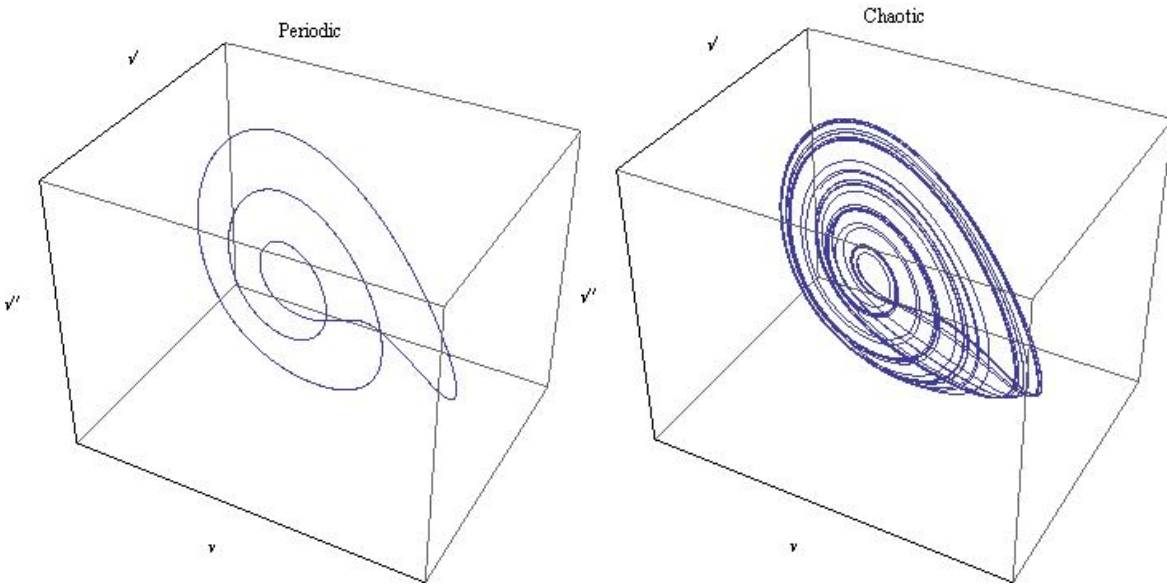


Figure 4: Three dimensional phase space created by allowing the orbit to evolve from the same initial conditions, for the same amount of time. Using a control parameter of 0.5061, we see periodic behavior (period 3 window, left) and using a control parameter of 0.5035, chaotic behavior is seen (right). In *Mathematica* 6, these plots can be rotated to examine characteristics of the phase space.

B. Modeled Lyapunov Exponent

Using the methods outlined in [1] a *Mathematica* algorithm was implemented to calculate the largest Lyapunov exponent. This algorithm was applied to our system and calculated within 1% of the value presented by [2] using a control parameter of 0.5.

Calculated Value:	.09404
Published Value:	.094
Fractional Difference:	1%

Since this algorithm calculated a largest Lyapunov exponent that agreed with the value reported, we considered it appropriately implemented and proceeded to calculate the largest Lyapunov exponent over a span of control parameter values. The spectra are presented in Figure 5, along with associated phase space diagrams in Figure 6. These figures show how the values of the largest Lyapunov exponent correspond with the behavior of the differential equation and the value of the control parameter.

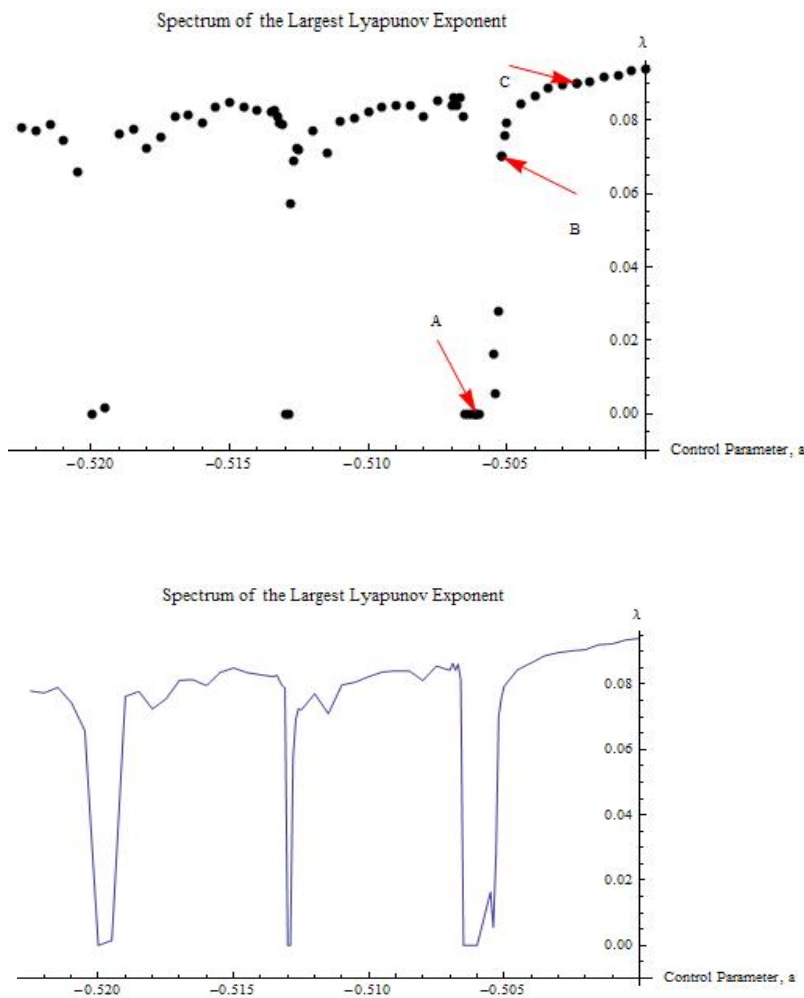


Figure 5: Data points of theoretical values for the largest Lyapunov exponent (top) are joined together to view a trend in the largest Lyapunov exponent. Points in labeled A, B, and C can be compared with phase space diagrams in Fig. 6. It is important to note that the spectra are shown with the negative of the control parameter values. In addition, the prominent dip near -0.506 corresponds to the “period three window.”

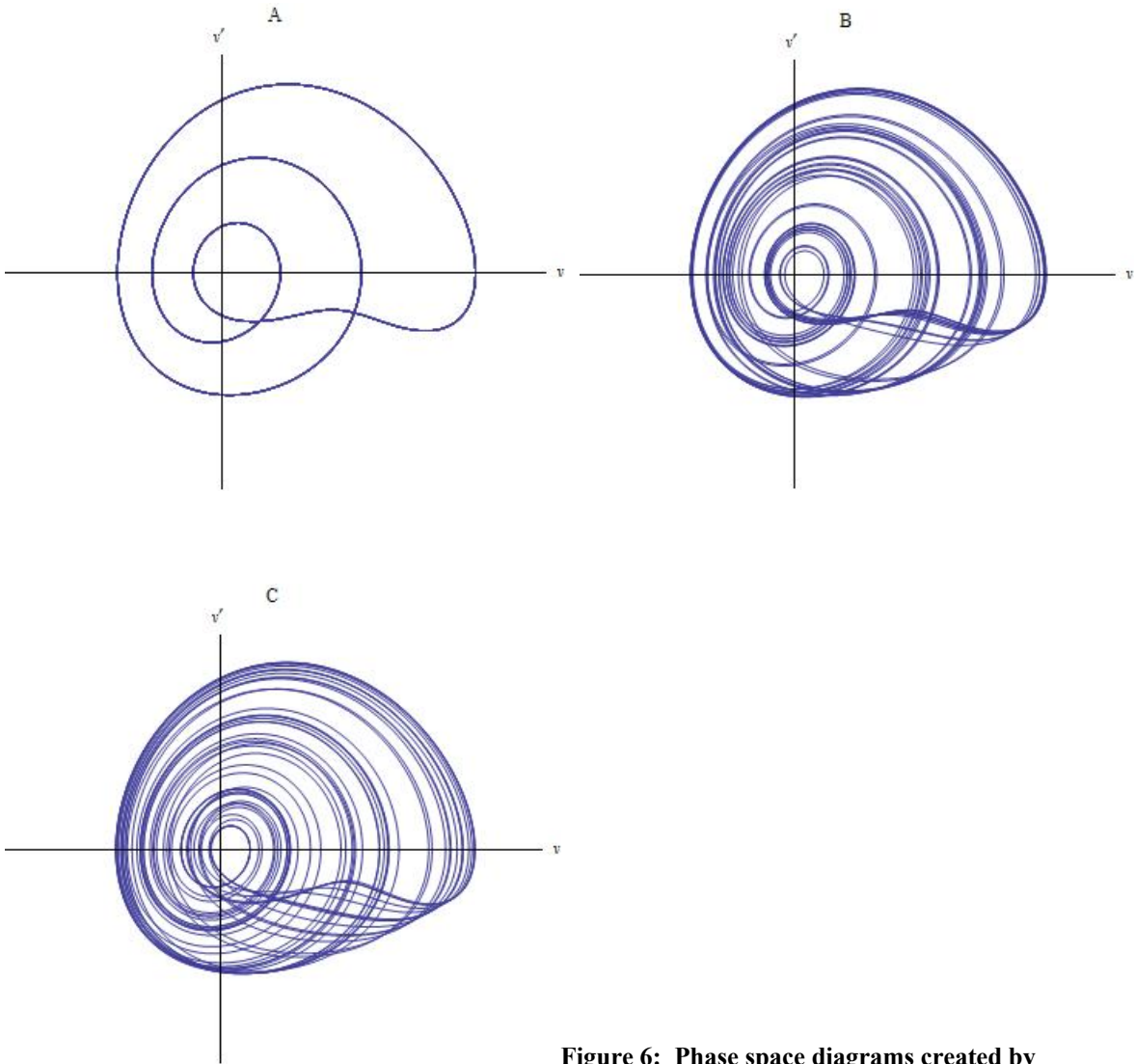


Figure 6: Phase space diagrams created by allowing the orbit to evolve from the same initial conditions, for the same amount of time. Control parameter values chosen correspond to the labeled arrows in Fig. 5 (top).

C. Phase Space Diagrams from Experimental Data

Time series data sets of (x,y,z) coordinates obtained from the circuit in Figure 1 and like those shown in the phase space diagrams in Figure 4 plotted parametrically as a function of time. These plots represent a three dimensional trajectory in the x , y , and z coordinates of Equation 3. A complete set of the phase plots over all values of the control parameter represents a complete characterization of the attractor of the chaotic system. Two examples of these phase plots for the period 3 window and for a value of the control parameter for which the system behaves chaotically are shown in Figures 7 and 8.

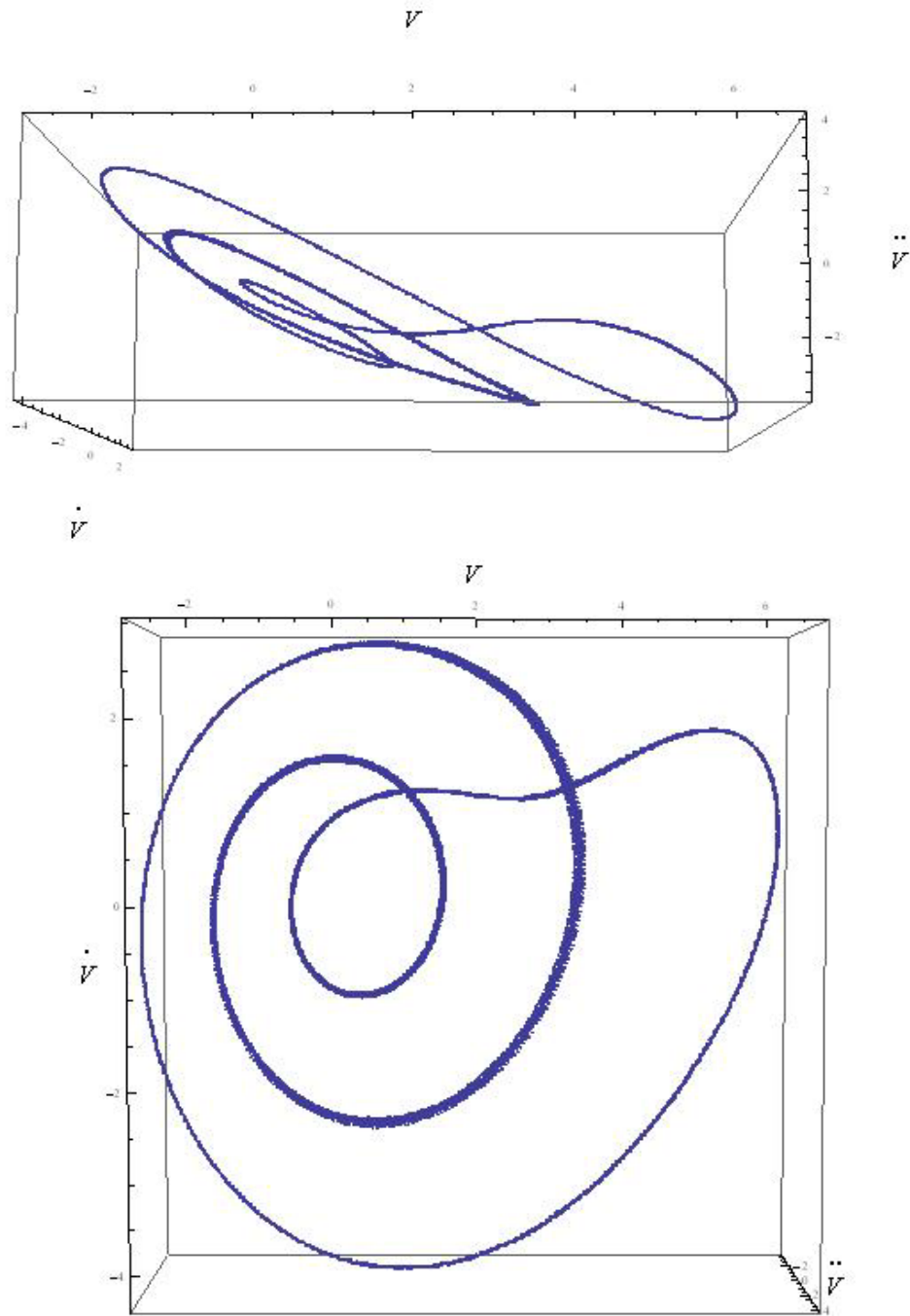


Figure 7: Two views of a 3-dimensional phase plot of the electronic circuit operating with a control voltage applied to the LM13700 VCR corresponding to the period 3 window. The features of these phase plots demonstrate good qualitative agreement with the modeled phase plots for the period 3 window shown in Figures 3 and 4.

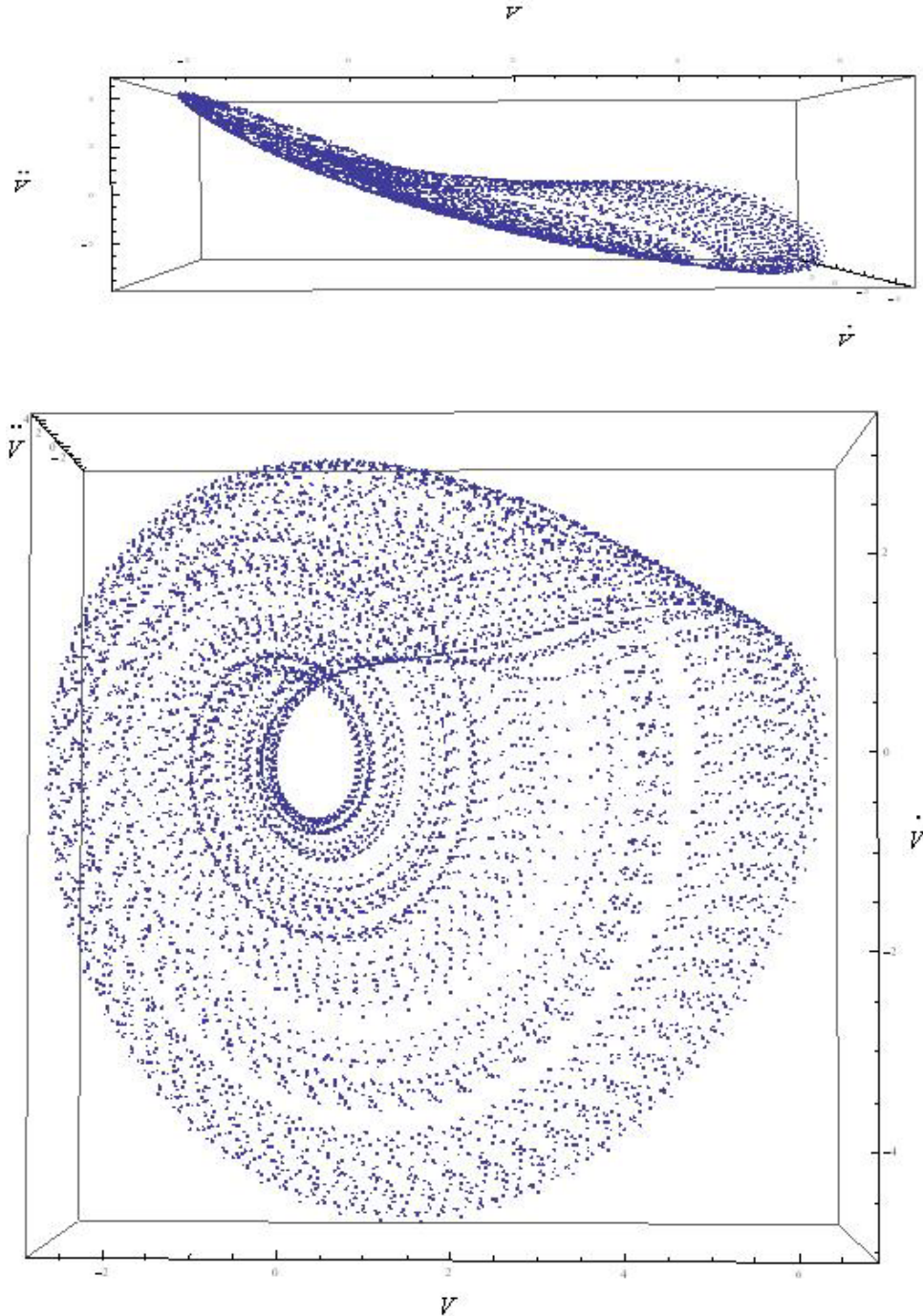


Figure 8: Two views of a 3-dimensional phase plot of the electronic circuit operating with a control voltage applied to the LM13700 VCR corresponding to chaotic behavior. The features of these phase plots demonstrate good qualitative agreement with the modeled phase plots for chaotic behavior shown in Figures 3 and 4.

D. Bifurcation in Experimental Attractor Data

A common feature of chaotic systems is behavior identified as bifurcation. Bifurcation occurs as the control parameter of a system is varied and the system responds

by a qualitative change in its attractor. Typically, the descent to chaos occurs as a control parameter is varied and these bifurcations occur at exponentially decreasing intervals of the control parameter. For systems that become chaotic by period doubling bifurcation this process is characterized by the Feigenbaum constant. Our system displays qualitative features consistent with the period doubling approach to chaos. We tried several approaches to experimentally characterizing the bifurcation process for our system but had difficulty because the control parameter intervals for bifurcations following the first four bifurcations were already very small, making it difficult to reproducibly distinguish subsequent bifurcations. Figure 9 displays phase plots of experimental data for several bifurcations displayed by our system.

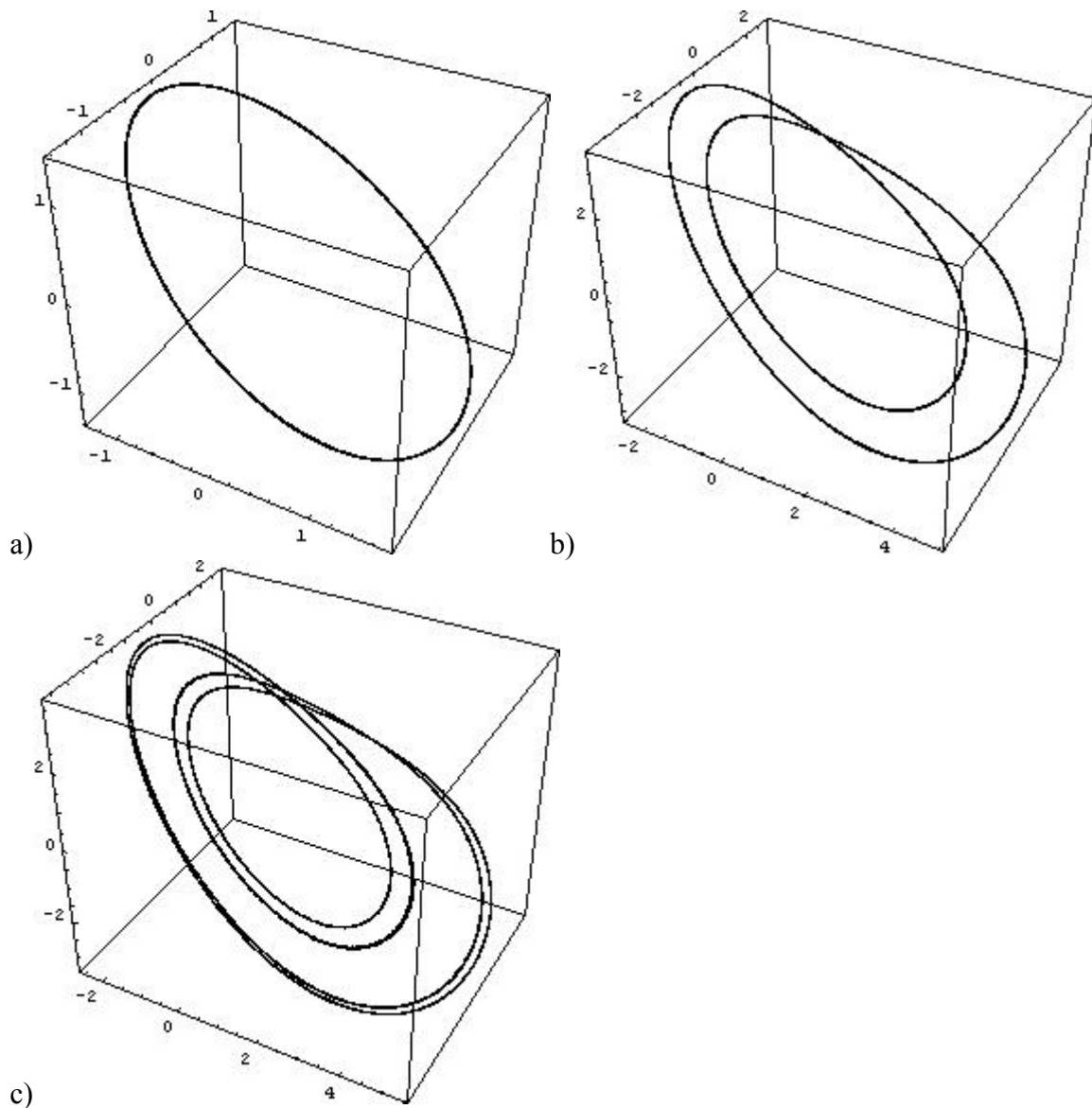


Figure 9: Three dimensional phase plots of experimental data collected at three different values of the control parameter apparently demonstrating period doubling bifurcation behavior. (a) The control

voltage applied to the LM13700 VCR is approximately $-4.75V$. This is referred to as the one-loop condition (b) The control voltage applied to the LM13700 VCR is approximately $-2V$. This is referred to as the two-loop condition (c) The control voltage applied to the LM13700 VCR is approximately $-1.5V$. This is referred to as the four-loop condition.

E. Experimental Lyapunov Spectrum

Time series data sets obtained from the circuit in Figure 1 and like those shown in the phase space diagrams in Figures 7 and 8 were used to obtain experimental values of the Lyapunov exponent over a range of control parameters. The scanned values of the control parameter included the period 3 window identified in Figures 3, 4, 5 and 6.

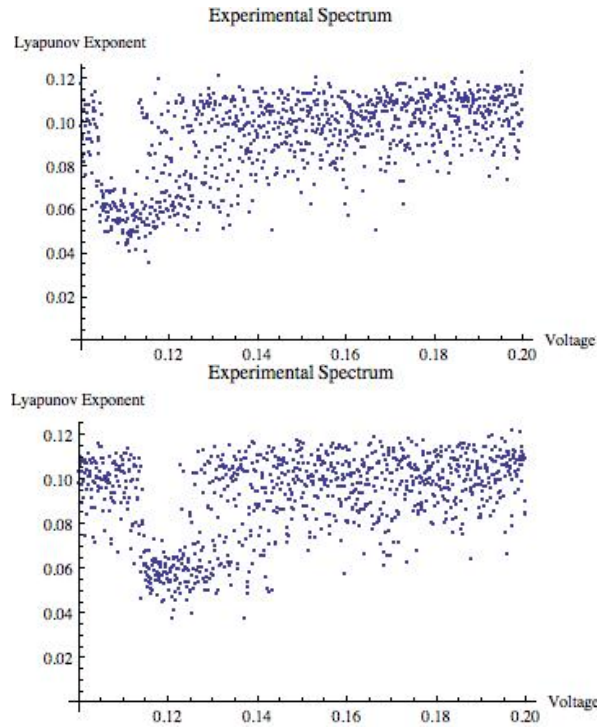


Figure 10: The Lyapunov exponent spectra shown above were calculated from two independent scans of the control parameter as described in section II. C. The value on the horizontal axis is the analog voltage applied to the LM13700 VCR by the DAQ, *not* the value of the control parameter. The broad dip in the value of the Lyapunov exponent centered near $V=0.11$ volts in the top spectrum and $V=0.12$ volts in the bottom spectrum are expected, as they correspond to the period 3 window identified in Figures 3, 4, 5 and 6. The broad scatter in the values of the Lyapunov exponent as a function of control parameter when compared to the modeled Lyapunov exponent spectrum shown in Figure 5 and the offset of the center of the period 3 window dip between the two spectra suggest that our techniques for experimentally measuring the Lyapunov exponent produce values that are not completely reproducible.

IV. Conclusions

Through computational investigations of Equation 2, we have found that it behaves both periodically and chaotically as would be expected from this form of nonlinear jerk

function. Analysis of Figures 5 and 6 show that the Lyapunov exponent predicts the behavior of Equation 2 by determining if chaos is present and how chaotically a system behaves. We also note the qualitative agreement of the Lyapunov exponent spectrum in the region around the period 3 window as shown in Figures 5 and 10. Typically, values of the Lyapunov exponent from experimental data were within 20% of values obtained from numerical modeling. Because the value of the largest Lyapunov exponent gives quantitative information about how chaotic a system behaves, we can observe that this can be qualitatively determined by how much area on the attractor is covered in a given amount of time (Figure 6). Despite the success of this algorithm, we suspect that the efficiency of the program could be increased for instance, by using a more efficient numerical approximation or by testing and exiting the program upon the convergence of a value, instead of processing for a constant number of iterations.

The qualitative agreement between Figures 3 and 4 with Figures 7 and 8 shows that the phase space characteristics predicted by numerical approximations were realized experimentally. Specifically, the period 3 window was physically observed, showing the electronic realization of our chaotic system. The data that was collected for this project did not allow a complete characterization of the LM13700 VCR control voltage – control parameter relationship, which limits the conclusions that can be reached about the quantitative agreement between our circuit and the numerical model. In addition, reproducibility for some aspects of circuit behavior proved difficult (see, for example Figure 10). We suspect that some of these issues could be reduced through addressing noise, sampling rates, sampling periods, and settling times.

With the work we have done on this project we are more convinced than ever that the systems identified in [2] are extraordinarily rich systems for introducing students to chaos. Among their features are that they provide opportunities for design, construction and troubleshooting of electronic circuits, numerical modeling, data acquisition, common and relatively easily demonstrable (other than the time series presented in this report, demonstrations of the chaotic behavior of these circuits can be achieved through oscilloscope displays and audio displays) characteristics of a range of chaotic behaviors, and that, because of the integrator-adder-gain design, all phase space coordinates of the system are accessible through measurement of voltages in the circuit. We highly recommend them to any physicists embarking on a study of chaotic systems.

V. Accounting of Funds

The CWU chapter of the Society of Physics Students gratefully acknowledges the resources that were provided by the National Society of Physics Students and the CWU Physics Department contributing to the success of this project. The Society of Physics Students Undergraduate Research Award allowed the CWU chapter of SPS to purchase necessary electronic equipment and components. In particular, all of the experimental data presented in this report was obtained with the National Instruments 6251 M-Series DAQ and from circuits constructed with discrete electronic components that were purchased with funds from the Award. The CWU Physics department provided a broad range of resources including computers and software for data acquisition and computational work, breadboards, electronic components, hookup wire, hand tools, lab space, and literature

resources. Equipment that has been purchased from the Undergraduate Research Award is identified in the list below.

National Instruments 6251 M-Series Data Acquisition hardware:	\$ 1261.72
Other discrete electrical components: (AD741, CA3140, AD734, LM13700, 1% Resistors, 1% Capacitors, Digital Potentiometers)	\$ 230.18

VI. Appendix

A. *Mathematica 6* code for the calculation of the largest Lyapunov exponent (control parameter is 0.5)

```

Clear["Global`*"]
R0 = {{0`20, 1`20, 0`20}};
dt = 1/100;
dr = {1/1010, 1/1010, 1/1010};
Rp = {Flatten[R0] + dr};
ARnorm = Norm[dr];
AR = {};
steps = 9 000 000;
a = 50/100;
Do[
  dr = ((Rp[[1]] - R0[[1]]) / Norm[Rp[[1]] - R0[[1]]]) * ARnorm;
  AppendTo[AR, dr];
  r1 =
  Flatten[
    NDSolve[{{x'[t] == y[t], y'[t] == z[t], z'[t] == -a z[t] - y[t] - x[t] + x[t]2,
      z[0] == R0[[1, 3]], y[0] == R0[[1, 2]], x[0] == R0[[1, 1]]}, {x, y, z},
      {t, 0, dt}, WorkingPrecision -> 20, PrecisionGoal -> 12, AccuracyGoal -> 12,
      StartingStepSize -> dt / 100];
  AppendTo[R0, {x[dt] /. r1, y[dt] /. r1, z[dt] /. r1}];
  rp =
  Flatten[
    NDSolve[{{x'[t] == y[t], y'[t] == z[t], z'[t] == -a z[t] - y[t] - x[t] + x[t]2,
      z[0] == R0[[1, 3]] + AR[[1, 3]], y[0] == R0[[1, 2]] + AR[[1, 2]],
      x[0] == R0[[1, 1]] + AR[[1, 1]]}, {x, y, z}, {t, 0, dt},
      WorkingPrecision -> 20, PrecisionGoal -> 12, AccuracyGoal -> 12,
      StartingStepSize -> dt / 100];
  AppendTo[Rp, {x[dt] /. rp, y[dt] /. rp, z[dt] /. rp}];
  R0 = Drop[R0, 1];
  Rp = Drop[Rp, 1];
  AR = Drop[AR, 1];
  /
  {n, 1, 1000 000}
]
λtot = Log[Norm[(Rp[[1]] - R0[[1]])] / ARnorm];
Do[
  dr = ((Rp[[1]] - R0[[1]]) / Norm[Rp[[1]] - R0[[1]]]) * ARnorm;
  AppendTo[AR, dr];
  r1 =
  Flatten[NDSolve[{{x'[t] == y[t], y'[t] == z[t],
      z'[t] == -a z[t] - y[t] - x[t] + x[t]2, z[0] == R0[[1, 3]],
      y[0] == R0[[1, 2]], x[0] == R0[[1, 1]]}, {x, y, z}, {t, 0, dt},
      WorkingPrecision -> 20, PrecisionGoal -> 12, AccuracyGoal -> 12,
      StartingStepSize -> dt / 100];
  AppendTo[R0, {x[dt] /. r1, y[dt] /. r1, z[dt] /. r1}];
  rp =
  Flatten[NDSolve[{{x'[t] == y[t], y'[t] == z[t],
      z'[t] == -a z[t] - y[t] - x[t] + x[t]2, z[0] == R0[[1, 3]] + AR[[1, 3]],
      y[0] == R0[[1, 2]] + AR[[1, 2]], x[0] == R0[[1, 1]] + AR[[1, 1]]},
      {x, y, z}, {t, 0, dt}, WorkingPrecision -> 20, PrecisionGoal -> 12,
      AccuracyGoal -> 12, StartingStepSize -> dt / 100];
  AppendTo[Rp, {x[dt] /. rp, y[dt] /. rp, z[dt] /. rp}];
  λtot = λtot + Log[Norm[(Rp[[1]] - R0[[1]])] / ARnorm];
  R0 = Drop[R0, 1];
  Rp = Drop[Rp, 1];
  AR = Drop[AR, 1];
  /
  {n, 1, steps}
];
λ = λtot / (steps * dt)

```

VII. References

1. J.C., Sprott, "Chaos and Time Series Analysis," Oxford University Press, 22-123 (2003).
2. J. C. Sprott, "Simple chaotic systems and circuits," *Am. J. Phys.* **68** (8), 758-763 (August 2000).
3. P. Horowitz, W. Hill, "The Art of Electronics" 2nd Ed, Cambridge University Press, 222 (1980).
4. Texas Instruments. "μA741 General-Purpose Operational Amplifiers," 2000.
<<http://www.us.oup.com/us/pdf/microcircuits/students/amps/ua741-ti.pdf>>
5. K. Kiers, D. Schmidt, J. C. Sprott, "Precision measurements of a simple chaotic circuit," *Am. J. Phys.* **72** (4), 503-508 (April, 2004).
6. Analog Devices. "AD734 10MHz, 4-Quadrant Multiplier/Divider," 1999.
<http://www.analog.com/UploadedFiles/Data_Sheets/AD734.pdf>
7. National Semiconductor. "LM13700 Dual Operational Transconductance Amplifiers with Linearizing Diodes and Buffers," 2004.
<<http://cache.national.com/ds/LM/LM13700.pdf>>
8. Kenneth A. Kuhn, "Practical Application of Op-Amps"
http://www.kennethkuhn.com/students/ee431/text/op_amp_practical_applications.pdf (2002).
9. M.T. Rosenstein, J.J. Collins, and C.J. De Luca. "A practical method for calculating largest Lyapunov exponents from small data sets," *Physica D* **65**, 117-134 (1993).
10. Wolfram Research Inc., Mathematica (1988-2007).